FEBS Letters 552 (2003) 68–73 FEBS 27551

Minireview

Mechanisms of membrane permeabilization by picornavirus 2B viroporin

José L. Nieva[a,*], Aitziber Agirre[a,1], Shlomo Nir[b], Luis Carrasco[c]

[a] *Unidad de Biofísica (CSIC-UPV/EHU) and Departamento de Bioquímica, Universidad del País Vasco, Aptdo. 644, 48080 Bilbao, Spain*
[b] *Seagram Center for Soil and Water Sciences, Faculty of Agricultural, Food and Environmental Quality Sciences, The Hebrew University of Jerusalem, Rehovot 76100, Israel*
[c] *Centro de Biología Molecular (CSIC-UAM), Universidad Autónoma de Madrid, Canto Blanco, 28049 Madrid, Spain*

Received 28 March 2003; revised 28 May 2003; accepted 2 June 2003

First published online 7 August 2003

Edited by Maurice Montal

Abstract Cell infection by picornaviruses leads to membrane permeabilization. Recent evidence suggests the involvement of the non-structural protein 2B in this process. We have recently reported the detection of 2B porin-like activity in isolated membrane–protein systems that lack other cell components. According to data derived from these model membranes, four self-aggregated 2B monomers (i.e. tetramers) would be sufficient to permeabilize a single lipid vesicle, allowing the free diffusion of solutes under ca. 1000 Da. Our findings also support a role for lipids in protein oligomerization and subsequent pore opening. The lipid dependence of these processes points to negatively charged cytofacial surfaces as 2B cell membrane targets.

Key words: Viroporin; Membrane permeabilization; Pore model; Poliovirus 2B

1. Introduction

Picornavirus-infected cells are good model systems for evaluating cell membrane alterations induced by viral infection. Picornavirus particles have components that permeabilize cells during virus entry. Macromolecules and other small compounds readily enter cells together with viral particles by a mechanism that is still undefined. After replication of the viral genome, the plasma membrane also becomes permeable to small solutes and ions. This late membrane alteration is accomplished by de novo synthesis of non-structural proteins by the virus. During the past few years, our understanding of the picornavirus components responsible for this late membrane disruption and their mode of action has greatly improved. For details on early work in this area the reader is referred to previous reviews [1,2].

2. Late membrane changes induced by picornaviruses

Picornaviruses induce a number of structural and functional alterations in cell membranes after infection. These alterations include an intense remodelling of intracellular membranes that inhibits the correct functioning of the vesicle system [2–4]. As a consequence, glycoprotein trafficking is hampered [5]. Intracellular membrane remodelling gives rise to numerous vesicles that are required for the replication of virus genomes [6–9].

The change in plasma membrane permeability to ions and solutes is another feature that, for several years now, has also received much attention [1,2]. As a result, this type of alteration has been described in detail. Compounds of MW less than 1000 Da are able to enter the cytoplasm from the mid phase of infection [10–14]. This passage of molecules occurs in both directions: from the cell interior to the culture medium and vice versa. The alterations that take place in cytoplasmic concentrations of monovalent cations provoke membrane depolarization, finally leading to cell lysis [10,14,15].

3. Picornavirus proteins involved in membrane alterations

Three non-structural viral proteins, 2B, 2BC and 3A, have the capacity to alter cell membranes when individually expressed in cells [5,16–22]. The three genes encoding these proteins are clustered in the picornavirus genome, which is expressed in the form of a long polyprotein precursor that is proteolytically cleaved by virus-encoded proteases. The 2BC precursor is the most active protein in terms of membrane alteration. 2BC shows certain activities that are not observed when 2B and 2C are co-expressed [16]. Nevertheless, several lines of evidence, including mutagenesis studies, suggest the capacity to enhance membrane permeability resides in the 2B moiety. Indeed, the synthesis of 2B alone disrupts membrane permeability in mammalian cells, although less efficiently than 2BC [5,17,20]. Perhaps the 2C protein serves to efficiently transport 2B to the plasma membrane. All three proteins, 2B, 2BC and 3A, enhance membrane permeability in prokaryotic cells [22]. However, in mammalian cells it has not yet been possible to associate 3A with this effect [17]. Perhaps, when individually expressed, this protein is retained in an intracellular compartment [8].

Finally, 2B, 2BC and, in an even more active manner, 3A are all able to impair glycoprotein trafficking through the vesicle system [5,16,18,19]. A component of this system lo-

*Corresponding author. Fax: (34)-94-601 3360.
E-mail address: gbpniesj@lg.ehu.es (J.L. Nieva).

[1] Present address: Elhuyar Foundation, 20170 Usurbil, Spain.

Abbreviations: CV, Coxsackie virus; GPA, glycophorin A; LUV, large unilamellar vesicles; PV, poliovirus; TMD, transmembrane domain

0014-5793/03/$22.00
doi:10.1016/S0014-5793(03)00852-4

```
CV-B          GVKDYVEQLGNAFGSGFTNQICEQVNLLKESLVGQDSILEKSLKALVKIISALVIVVRNH
HRV-14        GLSDYITGLGRAFGVGFTDQISTKVTELQE--VAKDFLTTKVLSKVVKMVSALVIICRNH
PV-2          GVSNYIESLGAAFGSGFTQQIGNKISELTS--MVTSTITEKLLKNLIKIISSLVIITRNY
PV-3          GISNYIESLGAAFGSGFTQQIGDKISELTS--MVTSTITEKLLKNLIKIISSLVIITRNY
PV-1          GITNYIESLGAAFGSGFTQQISDKITELTN--MVTSTITEKLLKNLIKIISSLVIITRNY
CV-A          GITSYIESLGTAFGAGFTHTISEKVTELTT--MVTSTITEKLLKNLVKIVSALVIVVRNY
HRV-2         GVTDYIHMLGEAFGNGFVDSVKEHIHAINP----VGNISKKIIKWMLRIISAMVIIIRNS
              *:..*:  ** *** **.. :  ::  :        . :  * :. :::::*::**: **

CV-B          DDLITVTATLALIGCTSSPWRWLKQKVSQYYGIPMAERQ 99
HRV-14        DDLVTVTATLALLGCDGSPWRFLKMYISKHFQVPYIERQ 97
PV-2          EDTTTVLATLALLGCDASPWQWLKKKACDILEIPYIMRQ 97
PV-3          EDTTTVLATLALLGCDVSPWQWLKKKACDTLEIPYVIRQ 97
PV-1          EDTTTVLATLALLGCDASPWQWLRKKACDVLEIPYVIKQ 97
CV-A          EDTTTILATLALLGCDISPWQWLKKKACDLLEIPHVMRQ 97
HRV-2         SDPQTILATLTLIGCSGSPWRFLKEKFCKWTQLNYIHKE 95
              .*  *: ***:*:**  ***::*:  ..  :   ::
```

Fig. 1. Multiple sequence alignment of picornavirus 2B protein sequences by CLUSTALW [48]. Conserved residues are indicated by the dots in the bottom row, while invariant residues are denoted by asterisks. Protein sequences: PV: poliovirus; CV: Coxsackie virus; HRV: human rhinovirus. Boxes designate hydrophobic domains.

cated at the endoplasmic reticulum may be the target for these proteins such that the Golgi apparatus becomes disorganized. The 2B product has been described to localize at the Golgi complex when expressed alone [23].

4. Structure of the 2B protein in membranes

Picornavirus 2B protein contains about 100 amino acids depending on the virus species considered (Fig. 1). Two hydrophobic regions have been identified in the protein [2,24–26]. At least one of these regions (poliovirus (PV)-1 2B residues ^{32}VTSTITEKLLKNLIKIISSLVIITG^{55}) could span the membrane by means of a partially amphipathic cationic helix (Figs. 1 and 2A,B). The second region (PV-1 2B residues ^{61}TTTVLATLALLGCDASPWQWL^{81}) is thought to be a transmembrane domain (TMD). Hydrophobicity distribution along the sequence seems to be functionally meaningful, since mutations altering either the first domain's amphipathicity or the second domain's hydrophobicity have been shown to interfere with the ability of 2B to increase permeability [17,20,21,25,27] and with viral RNA replication [24,25]. More recently, it has been reported that the occurrence of both domains in Coxsackie virus (CV) 2B mediates efficient Golgi targeting and plasma membrane permeabilization [23]. The presence of the two hydrophobic regions connected through a short stretch also suggests that in a putative oligomeric 2B aqueous pore, both domains would combine in each monomer to form a hairpin 'α-loop-α' motif spanning the bilayer [21,26]. In such a model, the amphipathic helix would subsequently serve to establish the interface between the lumen of the aqueous pore and the hydrophobic milieu of the membrane, and the second helix would span the bilayer as an integral transmembrane anchor (Fig. 2C). Integral hairpins would reverse chain direction, so that both the N- and the C-terminal ends of the polypeptide remain at the same side of the membrane.

The stability of the proposed 2B structure at membranes may be analyzed according to current understanding of the energetics of transmembrane helix insertion. Wimley and White's whole-residue hydrophobicity scale for partitioning into *n*-octanol provides a reasonable estimate of the free energy of inserting α-helical TMDs into bilayers [28,29]. The hydropathy plot in Fig. 2A was computed using octanol-to-water partitioning free energies (ΔG_{ow}), i.e. positive values in the plot denote a tendency to remain in the membrane-hydro-

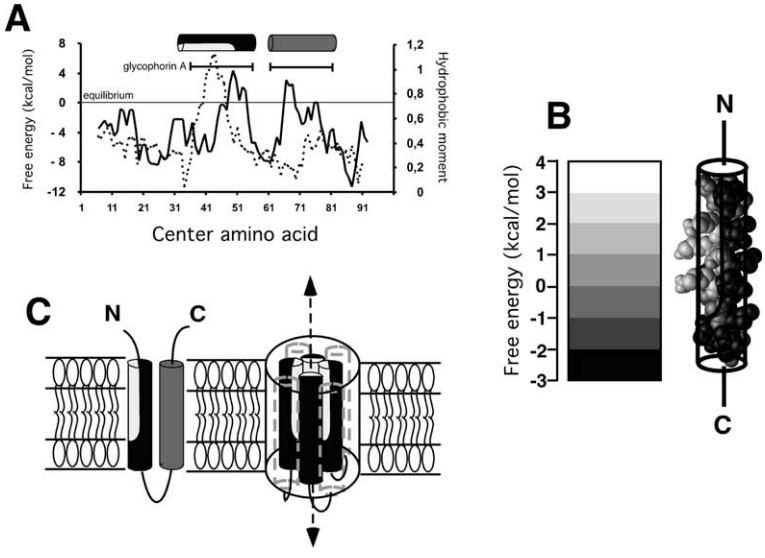

Fig. 2. A: Hydropathy plot revealing the hydrophobicity distribution within the PV-1 2B (primary sequence displayed in Fig. 1). For each central amino acid, the solid line represents the sum of Wimley–White's standard free energies of transfer (kcal/mol) from octanol to water (ΔG_{ow}) in windows of 11 residues (i.e. approximately three helical turns). The development of this scale is described in [28] and its use to evaluate the energetics of helix insertion into membranes is discussed in [29]. The dotted line corresponds to the average moment for a fixed $\delta = 100°$ and a similar amino acid window. The hydrophobic moment was calculated using the Eisenberg algorithm [49] with the modification that octanol-to-water transfer free energies for each amino acid were considered the moduli of the vectors that project from the main axes of the α-helix (see [50] for a detailed description). The cylinders above indicate the range and position of the proposed membrane-inserting domains. For comparative purposes, the length of a GPA TMD positive peak in a similar octanol-to-water free energy plot is also represented (*y*-axis values correspond to its maximum). B: Helical model for the PV-1 2B ^{32}VTSTITEKLLKNLIKIISSLVIITG^{55} sequence. Colors were graded according to the Wimley–White octanol scale as indicated in the side panel. C: Schematic models of PV-1 2B membrane structures. In the integral hairpin (left), the amphipathic 32–55 helix is shown with hydrophilic and hydrophobic sides in light gray and black, respectively, while the hydrophobic 61–81 helix is dark gray (according to insertion energy estimates, this structure is unlikely to be stable). The number of monomers in the transmembrane pore (right) was selected by mathematically modelling leakage assays (Table 1) and SDS–PAGE oligomer detection (Fig. 3). For better appreciation of central channel structure, the putative 61–81 TMD appears empty and is drawn in dashed lines.

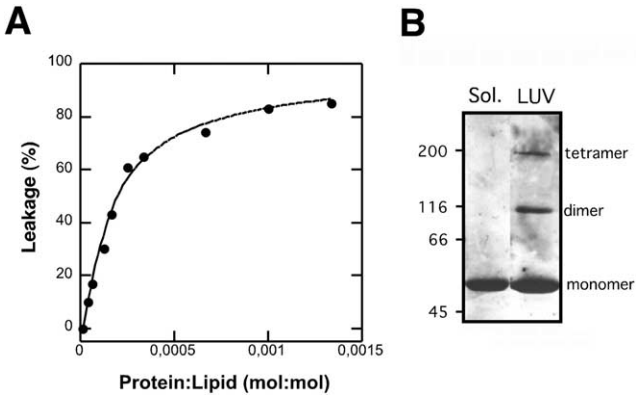

Fig. 3. Quaternary structure of PV-1 2B in membranes. A: Extent of aqueous content release (percentage maximum leakage at time = 60 min) induced by MBP-2B from phosphatidylinositol vesicles (ANTS/DPX assay) (circles). The solid line corresponds to the predicted curve calculated for a number of monomers required to permeabilize a vesicle M of 4 (see Appendix for mathematical model description). B: Oligomerization of 2B induced by its association with membranes. MBP-2B in solution (sol.) or mixed with LUV (protein-to-lipid molar ratio 1:1000) was incubated for 30 min and solubilized in SDS–PAGE sample buffer. The positions of the molecular weight markers are indicated.

carbon mimetic octanol phase. The PV-1 2B plot confirms the existence of two peaks above the 0 equilibrium value. However, compared to the canonical glycophorin A (GPA) TMD [29], 2B peaks are shorter in range (spanning six and three residues, respectively vs. 20 residues in GPA TMD) and are also less intense. Computing ΔG_{ow} values for the proposed bilayer-spanning PV-1 2B domains suggests that: (1) the 32–55 amino-domain would not spontaneously remain integrated within the membrane ($\Delta G_{ow} = -2.6$ kcal/mol), and (2) insertion of the 61–81 carboxy-domain would energetically be favored ($\Delta G_{ow} = 2.2$ kcal/mol) but the per-residue ΔG_{ow} value, 0.1 kcal/mol, is somewhat lower than that measured for stable anchors (~ 0.5 kcal/mol in GPA TMD [29]). Thus, our theoretical evaluation of the energy cost indicates the proposed hydrophobic domains would not allow the stable transmembrane insertion of 2B, at least as isolated helical anchors (Fig. 2C).

Hydrophobicity distribution may be considered in the context of an oligomeric pore. The hydrophobic moment analysis of PV-1 2B in Fig. 2A reveals that ca. two thirds of the hydrophobic amino-domain would generate one side with a strong affinity for membranes if folded as an α-helix (Fig. 2B). The V, I and L hydrophobes that are in contact with the hydrocarbon core would contribute to the amino-domain insertion energy to the extent of approximately 12.6 kcal/mol, or ca. 0.5 kcal/mol per residue. Thus, segregating hydrophilic residues towards the water-filled lumen of a putative pore would probably ensure the stable insertion of this domain in the membrane. This suggests that producing an integral amino-domain is causally linked to the establishment of a permeating oligomeric pore such as the one shown in Fig. 2C. On the other hand, stable insertion of the PV-1 2B carboxy-region seems to be hindered by the presence of several polar residues. Ion pairs and hydrogen-bonded polar residues are frequently used to drive the TMD association of integral membrane structures and constrain their conformations [30]. Similar interactions might decrease the polarity of the 2B carboxy-domain and contribute to the stability of the integral helical bundle. This hypothesis is to be experimentally contrasted in the near future using model systems (see Section 5).

5. Oligomerization and pore formation by 2B in model membranes

The ability of 2B to directly permeabilize membranes was assessed in a model system using large unilamellar vesicles (LUV) as substrates [26]. The experimental results point to the ability of 2B to induce the efflux of encapsulated solutes at low protein-to-lipid ratios (> 1:50 000). The molecular weight cut-off for the release of solutes was found to be approximately that of NADH (MW 660), whose Stokes radius is about 6 Å. These findings would appear to be consistent with the formation by viroporin 2B of a transmembrane pore that allows the free diffusion of small solutes. Thus, the process of 2B-induced membrane permeabilization lends itself to mathematical analysis according to a pore model (Fig. 3A, Table 1 and the Appendix).

The pore model assumes that vesicle-bound peptides self-aggregate. When an aggregate within a membrane has reached a critical size, i.e. it consists of M peptides, a pore can be created within the membrane, and leakage of encapsulated molecules can occur. It is also assumed that the process of peptide binding is rapid and once a pore has been formed in a vesicle, all its contents will quickly leak out. Since it is usually assumed that bound peptides do not interchange among vesicles, this leakage must be characterized by an all-or-none mechanism, i.e. the vesicle population will be comprised of those not leaking and those losing their entire contents. Further, the leakage process must end after a certain period to give a final extent of leakage, which depends on peptide-to-lipid ratios. The rate and extent of leakage are assumed to be limited by the rate and extent of formation of surface aggregates of M or more peptides. In most cases, surface aggregation of the peptides is not irreversible and depends on $K_s = C/D$, where C and D denote on and off rate constants of surface aggregation (see Appendix).

Our calculations using the variables M (pore size) and K_s, the degree of surface reversibility, include peptide binding and vesicle size distribution as input variables. The final extents of

Table 1
Final extents of leakage induced by the 2B peptide from phosphatidylinositol LUV

Lipid/protein (mol/mol)	Leakage (%)				
	Experimental	Calculated			
		$M = 2$ $K_S = 0.006$	4 0.05	6 0.1	8 0.2
750	85	83.6	86.9	84.3	85.1
1 000	83	79.8	83.6	80.5	81.4
1 500	74	73.3	77.7	73.8	75
2 000	78	68	72.7	68.1	69.5
3 000	65	59.6	64.3	58.9	60.2
4 000	61	53.1	57.5	51.4	52.4
6 000	43	43.8	46.9	39.7	39.4
8 000	30	37.3	38.8	30.9	29.3
16 000	17	23.2	19.8	11.9	8.5
25 000	10	15.5	10.3	4.4	2.2
100 000	0	2.9	0.3	0.02	0.001
R^2 =		0.96	0.98	0.97	0.97
RMSE		5.8	4	5.5	5.6

leakage are simulated as a function of peptide/lipid ratios. Table 1 shows experimental and calculated percentages of final extents of leakage from phosphatidylinositol LUV as a function of this ratio. Pore size (M) was noted to vary between $M=2$ and $M=8$. Best fits to the experimental results required larger K_s values for larger M values and vice versa. Thus, if the pore requires a small number of peptides, the presence of vesicles with more peptides than M is compensated in the calculations by a larger degree of reversibility of peptide surface aggregation, and vice versa. A close correlation between large K_s values and a large degree of irreversibility of formation of peptide surface aggregates was demonstrated for the peptides pardaxin [31], GALA [32] and the human immunodeficiency virus-1 (HIV-1) gp41 pretransmembrane sequence [33] by fluorescence assays that monitor self-quenching and energy transfer. The results in Table 1 indicate that best fitting to the experimental results is obtained for an assumed pore size $M=4$, the RMSE (root mean square error) increasing by 37.5, 40 and 45% when going from $M=4$ to $M=6$, 8 and 2, respectively. However, in each case, the values of R^2 are close to unity, and the values of RMSE may in fact be within the experimental error. Hence, values of $M=2$, 6 or 8 cannot be ruled out, despite the best fit for $M=4$. It still remains to be tested whether the pore model is insufficiently sensitive to account for pore size in the current system, or perhaps there is a wide pore size distribution in our case. In the study by Parente et al. [34], in which surface aggregation of the peptide GALA was essentially irreversible, the uncertainty in the deduced pore size ($M=10$) was less than 2 ($8 \leq M \leq 12$), and is consistent with the size of pre-encapsulated molecules that could leak out. This analysis therefore predicts that an oligomeric form of 2B, most likely a tetramer, is the permeating unit.

Initial evidence for 2B oligomerization was provided by studies on PV 2B variants that interfered with the replication of non-defective viruses [35]. Support for the idea that 2B forms homo-oligomers came from experiments using two-hybrid systems [36,37]. More recently, an elegant protocol based on fluorescence resonance energy transfer (FRET) microscopy in living cells has added further evidence to this notion in the case of CV 2B [38]. In a different but complementary approach, we found that non-radiant FRET between fluorescently labelled PV 2B-NBD and 2B-ANS occurs at the membrane surface but not in solution, indicating that oligomerization occurs in the membrane milieu [26]. Sodium dodecyl sulfate–polyacrylamide gel electrophoresis (SDS–PAGE) analysis provided further evidence that 2B is predominantly found as dimers and tetramers in membranes (Fig. 3B). This finding is in good agreement with the mathematical pore model predictions and points to tetramers as the permeating units. Of note is that SDS-resistant oligomer formation appeared to be promoted by membrane binding. Thus, membrane insertion probably helps set up interactions between 2B monomers that cannot be disrupted within the non-polar bilayer milieu, a requirement that must be fulfilled to assemble stable, functional pores.

Our findings using model membrane systems also seem to confirm the prediction that pore formation by 2B is probably concomitant to transbilayer integration (see Section 4). Recent experimental results obtained using LUV of defined composition indicate that water–membrane partitioning of soluble MBP-2B is mainly driven by electrostatic interactions (Agirre et al., unpublished observations). Negatively charged phospholipids promote insertion and oligomerization at the level of the membrane interface. However, the transition from surface-aggregated species to permeabilizing pores seems to be constrained by other conditions of the bilayer and specific protein residues. One bilayer property that seems to affect translocation and pore opening is the unsaturation degree of *sn*-2 acyl chains [26]. While negatively charged polar heads are probably required for surface association and coupled refolding, it is likely that acyl chain unsaturation provides conditions suitable for the conformational flexibility needed to perpendicularly insert 2B into the membrane. The same anionic phospholipids that modulate 2B pore formation in vitro preferentially localize at cytosol-facing membrane monolayers of different organelles including the Golgi apparatus [39]. Thus, the lipid-exerted regulation observed in model systems is basically in agreement with studies that pinpointed the Golgi body as a 2B target organelle [19,23].

6. Concluding remarks

Experimental results from model systems appear to be consistent with the formation by viroporin 2B of a transmembrane structure that allows free diffusion of small solutes. These findings support a molecular mechanism involving the direct permeabilizing action of 2B at the cell membrane. In monomers of the proposed membrane structure (Fig. 2C), three elements may be distinguished, namely, an amphipathic helix, a short connecting loop and a putative helical TMD. These might combine to form a hairpin 'α-loop-α' motif able to span the bilayer. The cationic amphipathic helix probably mediates interactions with anionic phospholipids. Lys/Arg-rich lytic amphipathic peptides, such as magainins or cecropins, preferentially bind to and permeabilize bilayers containing anionic phospholipids [40]. The mechanisms currently proposed for the formation of 'barrel-stave'-like pores by amphipathic sequences assume that, following rapid binding to membranes, aggregation occurs at their surface [41–44]. According to this rationale, a pore is formed when protein aggregates attain a critical size. Based on mathematical pore modeling (Table 1), this basic mechanism seems to be functional in the case of 2B.

The final assembly of the 2B permeating structure is likely to require the insertion of additional sequences into the membrane. Thus, 2B function is probably modulated by the second TMD helix and connecting loop adopting an adequate conformation and membrane topology. Short loops connecting transbilayer helices are common structural motifs in the permeating structures of channels belonging to the major intrinsic protein (MIP) family [45]. In addition, hydrophobic helices fully embedded in the membrane that reverse the chain direction have been found in channel proteins belonging to the mechanosensitive ion channel (MscL) family [46]. Atomic resolution of MscL proteins reveals that an amphipathic helix in each monomer serves to establish the interface between the lumen of the aqueous channel and the hydrophobic milieu of the membrane. A second helix provides an integral transmembrane anchor. The model in Fig. 2C suggests the same structural response for the 2B sequence, a bundle integrated within the membrane without translocation of the terminal ends of the molecule.

Ion channels such as those found in influenza and HIV-1

enveloped viruses also form homo-oligomers to create an ion flux across bilayers (see other articles in this issue). Remarkably, a membrane-embedded hairpin organization, oligomeric state and pore diameter, comparable to those described above for 2B, have been proposed for the membrane-inserting domain of *Bacillus thuringiensis* Cry1A toxin [47]. In summary, PV 2B protein might use structural themes common to those found in lytic peptides, integral channels and bacterial toxins to assemble tetrameric aqueous pores in membranes.

Acknowledgements: The authors gratefully acknowledge the financial support of the MCyT (EET 2001-1954), the Basque Government (PI-1999-7) and the University of the Basque Country (UPV 042.310-13552/2001) (grant awarded to J.L.N.) and DGICYT (PM99-0002) (grant awarded to L.C.). Also acknowledged is the institutional grant awarded to the Centro de Biología Molecular 'Severo Ochoa' by the Fundación Ramón Areces.

Appendix. Equations of pore model

The kinetics of irreversible aggregation was first investigated by Smoluchowski [51] and later extended to reversible aggregation [52]. The general scheme as treated in [53] is:

$$X_i + X_j \underset{D_{ij}}{\overset{C_{ij}}{\leftrightarrow}} X_{i+j} \tag{1}$$

where X_i is the molar concentration of an aggregate of order i; C_{ij} and D_{ij} are forward and backward rate constants of surface aggregation of the bound peptide. For simplicity and to avoid too many parameters, the calculations assumed $C_{ij} = C$ and $D_{ij} = D$. Here we have used the same scheme, but in our case X_i denotes surface concentration.

The fraction of encapsulated material that has leaked at the plateau level is denoted by L. Due to the dependence of the encapsulated volume on the third power of the inner diameter, a small fraction of large vesicles can contribute significantly to L. We consider the vesicles to consist of $j = 1,2,...S$ classes. The distribution of vesicles according to their diameters was determined by dynamic light scattering. We set $S = 10$ and we denote the fraction of encapsulated volume in vesicles of type j by f_j, $j = 1$–10 [31–33]. Let A_{ij} be the normalized fraction of vesicles of size class j that contain i bound peptides, i.e.

$$\sum_{i=0}^{N_j} A_{ij} = 1 \tag{2}$$

in which N_j is the largest number of peptides that can bind to a vesicle of size class j. The procedures for calculating the quantities A_{ij} from binding data have been described [54,55]. In the simpler case of irreversible surface aggregation of the peptide [34] the expression for L is given by

$$L = \sum_{j=1}^{S} \sum_{i=M}^{N_j} A_{i,j} f_j \tag{3}$$

Eq. 3 reflects the assumption that when aggregation is irreversible, all the peptides within the membrane will eventually be incorporated into a single aggregate so that all vesicles with at least M bound peptides will eventually leak. In the more general case of reversible surface aggregation the expression for L becomes

$$L = \sum_{j=1}^{S} \sum_{i=M}^{N_j} Z(M,i,j,K_S) A_{i,j} f_j \tag{4}$$

in which $Z(M,i,j,K_S)$ is the probability that a vesicle of size class j that contains i bound peptides will include an aggregate consisting of M or more peptides and K_S is given by

$$K_S = C/D \tag{5}$$

In the case of irreversible surface aggregation K_S tends to infinity. For the calculation of final extents of aggregation only K_S and the surface concentration of the peptides, X_0, are required, the latter being known from the binding measurements. As in [31]

$$Z = p^{M-1} x(M - Mp + p) \tag{6}$$

in which p is given by [52]

$$p = 1/(K + \sqrt{K^2 - 1}) \tag{7}$$

where K is given by

$$K = 1 + 1/(4K_S X_o) \tag{8}$$

For an infinite K_S the quantities K, p and Z equal unity and Eq. 4 reduces to Eq. 3, which corresponds to irreversible surface aggregation.

References

[1] Carrasco, L. (1995) Adv. Virus Res. 45, 61–112.
[2] Carrasco, L., Guinea, R., Irurzun, A. and Barco, A. (2002) in: Molecular Biology of Picornavirus (Semler, B.L. and Wimmer, E., Eds.), pp. 337–354, ASM Press, Washington, DC.
[3] Egger, D., Gosert, R. and Bienz, K. (2002) in: Molecular Biology of Picornavirus (Semler, B.L. and Wimmer, E., Eds.), pp. 247–253, ASM Press, Washington, DC.
[4] Cho, M.W., Teterina, N., Egger, D., Bienz, K. and Ehrenfeld, E. (1994) Virology 202, 129–145.
[5] Doedens, J.R. and Kirkegaard, K. (1995) EMBO J. 14, 894–907.
[6] Guinea, R. and Carrasco, L. (1990) EMBO J. 9, 2011–2016.
[7] Bienz, K., Egger, D., Pfister, T. and Troxler, M. (1992) J. Virol. 66, 2740–2747.
[8] Suhy, D.A., Giddings Jr., T.H. and Kirkegaard, K. (2000) J. Virol. 74, 8953–8965.
[9] Rust, R.C., Landmann, L., Gosert, R., Tang, B.L., Hong, W., Hauri, H.P., Egger, D. and Bienz, K. (2001) J. Virol. 75, 9808–9818.
[10] Carrasco, L. and Smith, A.E. (1976) Nature 264, 807–809.
[11] Carrasco, L. (1978) Nature 272, 694–699.
[12] Contreras, A. and Carrasco, L. (1979) J. Virol. 29, 114–122.
[13] Irurzun, A., Perez, L. and Carrasco, L. (1993) J. Gen. Virol. 74, 1063–1071.
[14] Lacal, J.C. and Carrasco, L. (1982) Eur. J. Biochem. 127, 359–366.
[15] Schaefer, A., Kuhne, J., Zibirre, R. and Koch, G. (1982) J. Virol. 44, 445–449.
[16] Barco, A. and Carrasco, L. (1995) EMBO J. 14, 3349–3364.
[17] Aldabe, R., Barco, A. and Carrasco, L. (1996) J. Biol. Chem. 271, 23134–23137.
[18] Doedens, J.R., Giddings Jr., T.H. and Kirkegaard, K. (1997) J. Virol. 71, 9054–9064.
[19] Sandoval, I.V. and Carrasco, L. (1997) J. Virol. 71, 4679–4693.
[20] Van Kuppeveld, F.J.M., Hoenderop, J.G.J., Smeets, R.L.L., Willems, P.H.G.M., Kijkman, H.B.P.M., Galama, J.M.D. and Melchers, W.J.G. (1997) EMBO J. 16, 3519–3532.
[21] Van Kuppeveld, F.J.M., Melchers, W.J.G., Kirkegaard, K. and Doedens, J.R. (1997) Virology 227, 111–118.
[22] Lama, J. and Carrasco, L. (1992) J. Biol. Chem. 267, 15932–15937.
[23] De Jong, A.S., Wessels, E., Dijkman, H.B., Galama, J.M., Melchers, W.J., Willems, P.H. and Van Kuppeveld, F.J. (2003) J. Biol. Chem. 278, 1012–1021.

[24] Van Kuppeveld, F.J.M., Galama, J.M.D., Zoll, J. and Melchers, W.J.G. (1995) J. Virol. 69, 7782–7790.
[25] Van Kuppeveld, F.J.M., Galama, J.M.D., Zoll, J., Van den Hurk, P.J.J.C. and Melchers, W.J.G. (1996) J. Virol. 70, 3876–3886.
[26] Agirre, A., Barco, A., Carrasco, L. and Nieva, J.L. (2002) J. Biol. Chem. 277, 40434–40441.
[27] Barco, A. and Carrasco, L. (1998) J. Virol. 72, 3560–3570.
[28] Wimley, W.C. and White, S.H. (1996) Nat. Struct. Biol. 3, 842–848.
[29] White, S.H., Ladokhin, A.S., Jayasinghe, S. and Hristova, K. (2001) J. Biol. Chem. 276, 32395–32398.
[30] Zhou, F.X., Merianos, H.J., Brunger, A.T. and Engelman, D.M. (2001) Proc. Natl. Acad. Sci. USA 98, 2250–2255.
[31] Rapaport, D., Peled, R., Nir, S. and Shai, Y. (1996) Biophys. J. 70, 2503–2512.
[32] Nicol, F., Nir, S. and Szoka Jr., F.C. (1996) Biophys. J. 71, 3288–3301.
[33] Sáez-Cirión, A., Nir, S., Lorizate, M., Agirre, A., Cruz, A., Pérez-Gil, J. and Nieva, J.L. (2002) J. Biol. Chem. 277, 21776–21785.
[34] Parente, R.A., Nir, S. and Szoka, F.C.Jr. (1990) Biochemistry 29, 8720–8728.
[35] Wimmer, E., Hellen, C.U. and Cao, X. (1993) Annu. Rev. Genet. 27, 353–436.
[36] Cuconati, A., Xiang, W.K., Lahser, F., Pfister, T. and Wimmer, E. (1998) J. Virol. 72, 1297–1307.
[37] De Jong, A.S., Schrama, I.W., Willems, P.H., Galama, J.M., Melchers, W.J. and Van Kuppeveld, F.J. (2002) J. Gen. Virol. 83, 783–793.
[38] Van Kuppeveld, F.J., Melchers, W.J., Willems, P.H. and Gadella Jr., T.W. (2002) J. Virol. 76, 9446–9456.
[39] Sprong, H., van der Sluijs, P. and van Meer, G. (2001) Nat. Rev. 2, 504–513.
[40] Matsuzaki, K. (1998) Biochim. Biophys. Acta 1376, 391–400.
[41] Shai, Y. (1995) Trends Biochem. Sci. 20, 460–464.
[42] Bechinger, B. (1997) J. Membr. Biol. 156, 197–211.
[43] Nir, S. and Nieva, J.L. (2000) Prog. Lipid Res. 39, 181–206.
[44] Huang, H.W. (2000) Biochemistry 39, 8347–8352.
[45] Fu, D., Libson, A., Miercke, L.J., Weitzman, C., Nollert, P., Krucinski, J. and Stroud, R.M. (2000) Science 290, 481–486.
[46] Chang, G., Spencer, R.H., Lee, A.T., Barclay, M.T. and Rees, D.C. (1998) Science 282, 2220–2226.
[47] Masson, L., Tabashnik, B.E., Liu, Y.B., Brousseau, R. and Schwartz, J.L. (1999) J. Biol. Chem. 274, 31996–32000.
[48] Thompson, J.D., Higgins, D.G. and Gibson, T.J. (1994) Nucleic Acids Res. 22, 4673–4680.
[49] Eisenberg, D., Weiss, R.M. and Terwilliger, T.C. (1982) Nature 299, 371–374.
[50] Sáez-Cirión, A., Gómara, M.J., Agirre, A. and Nieva, J.L. (2003) FEBS Lett. 533, 47–53.
[51] Smoluchowski, M.V. (1917) Phys. Chem. (Leipzig) 92, 129–168.
[52] Blatz, P.J. and Tobolsky, A.V. (1945) J. Phys. Chem. 49, 77–80.
[53] Bentz, J. and Nir, S. (1981) Proc. Natl. Acad. Sci. USA 78, 1634–1637.
[54] Nir, S., Klappe, K. and Hoekstra, D. (1986) Biochemistry 25, 2155–2161.
[55] Bentz, J., Nir, S. and Covell, D.G. (1988) Biophys. J. 54, 449–462.